5-2004

Self-Assembly of Inorganic Membranes: Attachment of Gold Nanoparticles to a Mesoporous Silica Membrane

Jennifer K. Saucier

SELF-ASSEMBLY OF INORGANIC MEMBRANES: ATTACHMENT OF GOLD NANOPARTICLES TO A MESOPOROUS SILICA MEMBRANE

by

Jennifer K. Saucier

A Thesis Submitted in Partial Fulfillment
Of the Requirements for a Degree with Honors
(Chemical Engineering)

The Honors College

University of Maine

May 2004

Advisory Committee:

Dr. Michael Boyle, Associate Professor of Mechanical Engineering, Honors College
Dr. William DeSisto, Assistant Professor of Chemical and Biological Engineering, Advisor
Dr. David Neivandt, Assistant Professor of Chemical and Biological Engineering and Director of Product Development
Sharon Tisher, Resource Economics and Policy, Honors College
Dr. M. Clayton Wheeler, Assistant Professor of Chemical and Biological Engineering

Acknowledgements

There are many people that I would thank for their contributions to my thesis project. Without their help and commitment I would not have been able to complete this endeavor.

Dr. William DeSisto: Thank you very much for all of your help as an Advisor for this project. You are always willing and excited to assist me in completing this project while welcoming me into your lab.

My thesis committee Dr. Michael Boyle, Dr. David Neivandt, Sharon Tisher, Dr. M. Clayton Wheeler: Thank you for all your help and commitment to this project through recommendations and words of encouragement.

Scott Higgins: Scott, thank you for being my super lab buddy. I really enjoyed all of the fun we had while working through our projects.

Nick Hill: Nick, thank you for helping me work with all of the equipment in the lab through your patient training!

Dr. Alla Gamarnik: Thank you for all of your patience in working with me to operate and use your trough and facilities. Your dedication and time commitment over Spring Break is especially appreciated!

Robert Fisher: Thank you for taking time out of your schedule to create my dipping apparatus (and re-creating it!)

My Family and Friends: Throughout the years you have all been a great support system and inspiration to me. You have put up with me throughout the course of both this project and my education, through the ups and downs. Thank you for all your encouragement!

Abstract

The purpose of this study was to investigate the self-assembly of gold nanoparticles to create thin, densely packed structures several monolayers thick for the synthesis of a membrane. Silica membrane synthesis was examined as a support for deposition of the nanoparticles. Pore size formation and thickness were controlled to promote high flux, defect free layer formation while providing for optimum separation.

Silica mesoporous membranes were created through the acid-catalyzed hydrolysis of tetraethyl orthosilicate. An ionic block co-polymer was used to control a networked pore formation. The silica sols were dip coated on macroporous alumina supports. The silica membranes were characterized through gas permeance testing and determined to have a pore formation in the mesoporous range. The films were found to be defect free and thin resulting in a high flux through the membrane. Multi-gas testing indicated that flux is inversely proportional to the inverse square root of temperature.

Gold Nanoparticles were synthesized at an estimated 15+/-2nm in diameter. The gold nanoparticles were plated in a multi-layered packing arrangement onto the silica membranes using a Langmuir-Blodgett dipping technique. Characterization of the disks was completed. The gold nanoparticle films were found to have a high permeance indicating a thin membrane.

List of Tables

List of Figures

Table of Contents

1. Introduction

1.1 Porous Inorganic Membranes

The use of inorganic membranes has become popular due to their potential for various applications. These membranes have the ability to operate in a broad range of temperatures and have an extensive long-term stability. In addition, inorganic membranes can hold up to significant differences in pressure and have a large surface area to volume ratio [1]. Since organic membranes do not hold up well in harsh or corrosive environments, inorganic membranes have provided a whole new means for separation in those areas [2].

Membranes are devices that are permeable in a selective manner to create a separation between one or more liquids or gases as shown in Figure 1 [2]. Membranes create a barrier that prevent mixing or contact between components. For this barrier to be effective it must have a selective permeability [1].

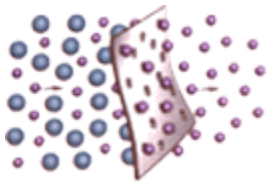

Figure 1 **-** Membrane separation- Membranes are used to separate gases and liquids in a variety of processes [2]

In general membranes are constructed in a layered format as shown in Figure 2. The bottom layer, a support structure, is usually chosen due to its large pore size. The support is coated with successively smaller layers that decrease in pore size. The layer that is placed on top is in contact with the medium to be separated [1]. This layer has the

smallest pore size to provide for optimal separation and is commonly referred to as the critical separation layer. This layer can be composed of one or many small layers with the top layer being very thin to allow for the maximum permeance [2].

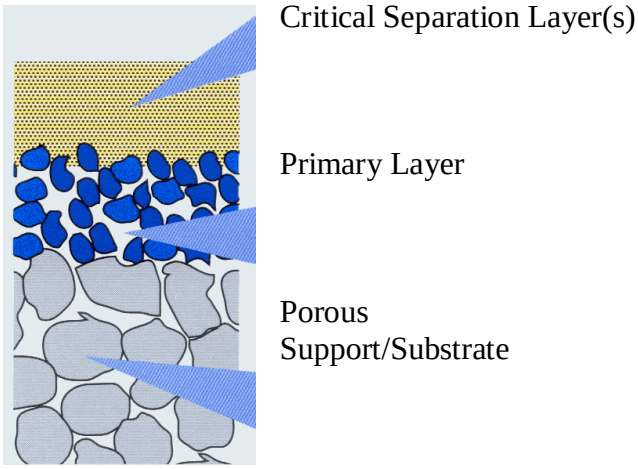

Figure 2 - Layered membrane system to provide for decreased pore size and greater separation technologies [2].

Different materials such as polycrystalline zeolite, sol-gel silica and amorphous carbon fulfill many of the demands in membrane technology by covering a wide range of diffusivities. These materials are appropriate for various gaseous or liquids due to pore size formation [3]. Inorganic membranes are found to be applicable in many separation systems. Materials such as these have been very helpful to the control pore size and shape. Applications of these inorganic membranes include chemical sensing, shape-selective catalysis, molecular sieving, and selective absorption [4]. Other common applications include reverse osmosis, membrane reactors and gas separations [1].

1.2 Macroporous Support Membranes

Macroporous membranes are characterized by a pore diameter greater than 50nm. Macroporous supports are generally ceramic membranes that are used as a base for successive deposition of membrane layers. Macroporous ceramic supports are made by shaping a powder and sintering the resulting unit to create a consolidation of the material. Various techniques can be applied to create a macroporous support. The most common techniques available are extrusion and tape casting [1].

The sintered supports can be characterized through the use of gas permeation. The macroporous membrane is differentiated by gas flow that follows the Hagen-Poiseuille equation.

$$J \equiv \frac{r^2 \cdot \varepsilon \cdot \Delta P \cdot P_{ave}}{8 \cdot \eta \cdot \tau \cdot \Delta x} \qquad \text{(Eq. 1)}$$

The flux, J, is determined from the relationship between the membrane thickness, Δx, and the change in pressure across the membrane, ΔP. The other variables of interest include the porosity of the disk, ε, viscosity, η, tortuosity, τ, and radius, r. The Hagen-Poisueille equation can be used to describe the laminar flow of a gas [5]. Macroporous membranes are characterized by gas permeation that depends on pressure as seen with Poiseuille's Equation. The permeance is defined by Equation 2.

$$Permeance \equiv \frac{J}{\Delta P} \qquad \text{(Eq. 2)}$$

The resulting permeance is related to pressure through the proportionality

$$Permeance \propto \frac{\varepsilon}{8 \cdot \eta \cdot \tau} \cdot \frac{r^2}{R \cdot T \cdot L} \cdot P_m \qquad \text{(Eq. 3)}$$

The width of the film, L, gas constant, R, temperature, T, and pressure, P_m, are taken into consideration in the equation.

1.3 Mesoporous Membranes

Mesoporous membranes are characterized by a pore diameter from 2-50nm [1]. These sol-gel membranes are created by using a dip-coating technique. Most silica membranes are prepared as a silica sol that is dip-coated on an adequate macroporous support. The majority of membranes incorporate tetraethylorthosilicate (TEOS) and ethanol to create the silica network around a surfactant through an acid-catalyzed hydrolysis and condensation reaction [3].

The basis of formation of a sol-gel silica membrane is the network formation that occurs around the surfactant. The network formed through a condensation reaction creates a structured form. Through the addition of a surfactant, pores can form within the networked structure. Micelles are self-assembled amphiphilic structures that assemble due to hydrophobic interactions between surfactant molecules. The interior of the micelle consists of the hydrophobic ends of the molecule while the outside surface is the

hydrophilic head groups. This structure prevents unfavorable interactions within the silica network. A picture of a micelle can be seen in Figure 3.

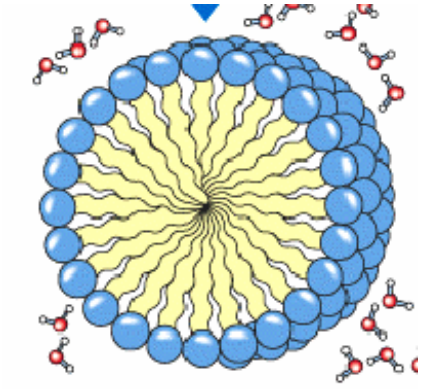

Figure 3 - A micelle formed through favorable hydrophobic interations between surfactant molecules. Hydrophilic head groups form the outside layer of the structure as a barrier [6].

Inorganic films can form into various mesoporous structural networks. Extensive research has indicated that one of three pore formations can occur: hexagonal, lamellar, and cubic. Hexagonal mesophases are a one dimensional system of cylindrical pores arranged in a hexagonal packing. Cubic structure is characterized by a three dimensional system of interconnected pores. A lamellar structure is a two dimensional bilayer system of surfactant with exterior metal oxide sheet formation [7]. The resultant structure of a membrane can be altered by changing the volume fraction of block copolymer present in the sol [8]. Figure 4 presents a schematic of the different packing structures.

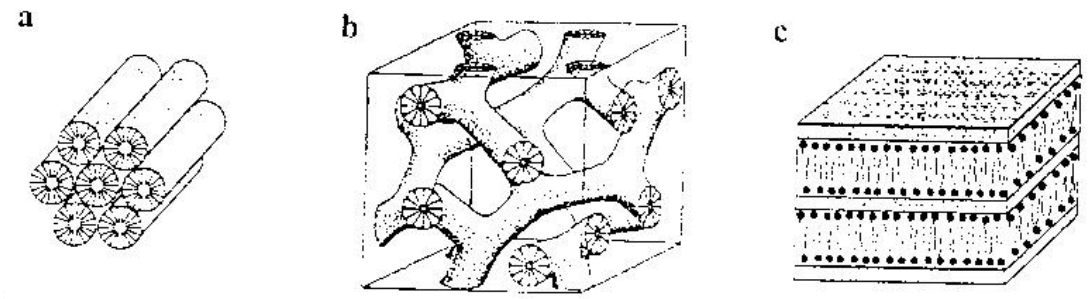

Figure 4 **–** Hexagonal, cubic, and lamellar packing structures that can be created within organic membranes. a) hexagonal b) cubic c) lamellar [7]

These mesoporous structures have the ability to perform gas separations due to their restricted pore size. This selectivity results from Knudsen Diffusion of the gas particles. Knudsen Diffusion is the lack of interactions between gas particles while flow and diffusion are fundamentally the same [1].

$$\lambda \equiv \frac{k \cdot T}{\pi \cdot d_{gas}^{2} \cdot P \cdot \sqrt{2}} \qquad \text{(Eq. 4)}$$

where T is temperature, d_{gas} is the diameter of the respective gas molecules, and k is Plank's constant.

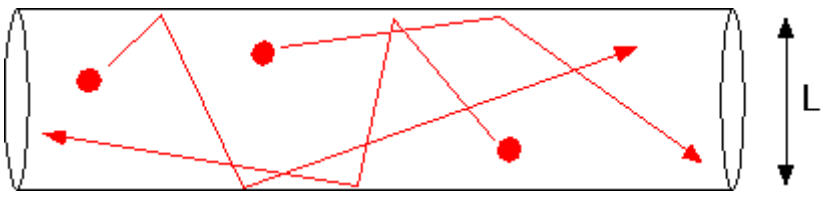

Figure 5 - Knudsen Diffusion as characterized by the infrequent collision between gas molecules and pore walls [9].

The flux, J, of the mesoporous membrane is characterized for species i by the equation:

$$J_i \equiv \frac{\pi \cdot n \cdot r^2 \cdot D_k \cdot \Delta P}{R \cdot T \cdot \tau \cdot L} \qquad \text{(Eq. 5)}$$

where τ is tortousity, n is the number of moles, L is the membrane thickness, and D_k is the Knudsen Diffusion coefficient. This coefficient is defined by the equation:

$$D_k \equiv .\frac{.66 \cdot r \cdot R \cdot T^{.5}}{\tau \cdot M^{.5}} \qquad \text{(Eq. 6)}$$

where M is the molecular weight of a particular gas i. Through derivation of the flux for two gases in separation, the ideal Knudsen separation factor for two gases of different molecular weights would be defined by:

$$\alpha \equiv \sqrt{\frac{M_1}{M_2}} \qquad \text{(Eq. 7)}$$

Where M_1 and M_2 are the molecular weights of gas one and gas two respectively [10].

Mesoporous membranes as characterized by Knudsen flow have a permeance that is dependent on the molecular weight of a gas as defined by:

$$Permeance \propto \frac{2 \cdot \varepsilon \cdot r}{3 \cdot \tau \cdot \theta_k \cdot L} \cdot \left(\frac{8}{\pi \cdot R \cdot T \cdot M} \right)^{.5} \qquad \text{(Eq. 8)}$$

This proportionality indicates that Knudsen flow in mesoporous membranes has no dependence on pressure.

The original permeance values must be found for both the macroporous substrate and film combined. To determine the permeance values for solely the mesoporous film the

permeance of the support must be removed from the total permeance value. The permeance of the disk is subtracted off by using Equation 9.

$$\frac{1}{P_{diskandfilm}} \equiv \frac{1}{P_{disk}} + \frac{1}{P_{film}} \qquad \text{(Eq. 9)}$$

From this data the permeance values can be used to determine the pore structure of the film

1.4 Microporous Membranes Composed of Nanoparticles

Microporous membranes are distinguished by a pore diameter that is less than 2nm. These microporous membranes have been created using a variety of materials and methods. Investigation has been completed of a unique synthesis of microporous membranes using the self-assembly of gold nanoparticles deposited on a sufficient mesoporous layer. This was accomplished through the use of Langmuir-Blodgett deposition.

The theory behind the Langmuir-Blodgett Trough was produced by a young woman named Agnes Pockel. Pockel developed a method of applying water-insoluble compounds to the surface of water based solution by dissolving the compound in an organic solvent. The solvent was then allowed to evaporate leaving the compound spread over the water surface [11]. With gold particles, an ionic attraction occurs between the negative gold nanoparticles and the positive water-insoluble compound. This causes the

molecules to rise to the surface and bind with the organic molecule. Figure 6 illustrates the layer formation at the air-water interface.

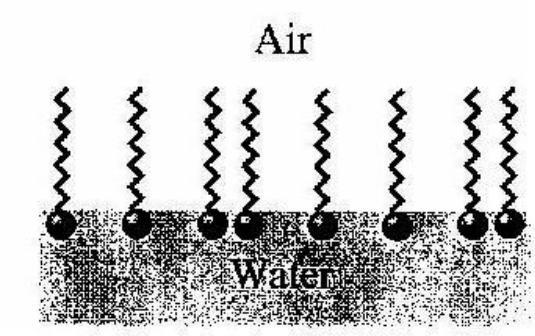

Figure 6 - Illustration of a monolayer spread over the air-water interface in a Langmuir Trough. [12]

By using the Langmuir-Blodgett trough the nanoparticles can be compressed into a monolayer. A compressed monolayer results when the distance between particles is the same size as the diameter of the particles. This point of compression is referred to as the "Pockel's Point" [13].

To create a multi-layer particle membrane the film must be compressed beyond the Pockel's Point. This decrease in the area available for the particles forces the particles to raft on top of each other. This rafting forms a multi-layered structure capable of being plated as a membrane [14]. The particles if layered in a perfect structure would form a cubic close-packed structure (ccp). A diagram of this packing formation can be seen in Figure 7.

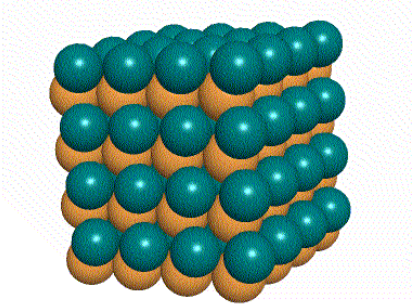

Figure 7 **-** Illustration of a cubic close-packed structure. This formation is anticipated for the nanoparticles in multi-layer formation [15].

It is anticipated that in this structured form gas flow will occur between the particles. Calculations can be performed using the cubic close-packed structure to determine a pore diameter for the multi-layered formation (please see Appendix A for calculations).

2. Synthesis and Characterization of Mesoporous Silica Membranes via Dip-Coating

2.1 Introduction

The purpose of this study was to find a thin inorganic sol-gel membrane to be used as a support structure on which to deposit gold nanoparticles. It was anticipated that an inorganic silica film would serve as a good deposition layer. Silica mesoporous membranes have applications in ultrafiltration and as supports for catalysts and microporous membranes. Silica mesoporous membranes have been fabricated by a variety of techniques using materials such as micellular aggregate templates, non-ionic surfactants [16]. The synthesis of mesoporous silica membranes was investigated using block copolymers as structure directing agents.

2.2 Experimental

2.2.1 SYNTHESIS

2.2.1.1 Creation of Silica Sol-Gel

Mesoporous silica membranes were prepared using a formula as described by Alberius et. al. The reaction mechanism for this particular solution involves an acid catalyzed hydrolysis reaction of tetraethylorthosilicate (TEOS) with water. The hydrolysis replaces one side group of each TEOS molecule with a hydroxyl functional group. A bond forms between two of the TEOS molecules through a condensation reaction. Continued hydrolysis promotes the formation of a complete silica network. The chemical reactions are shown in Figure 8.

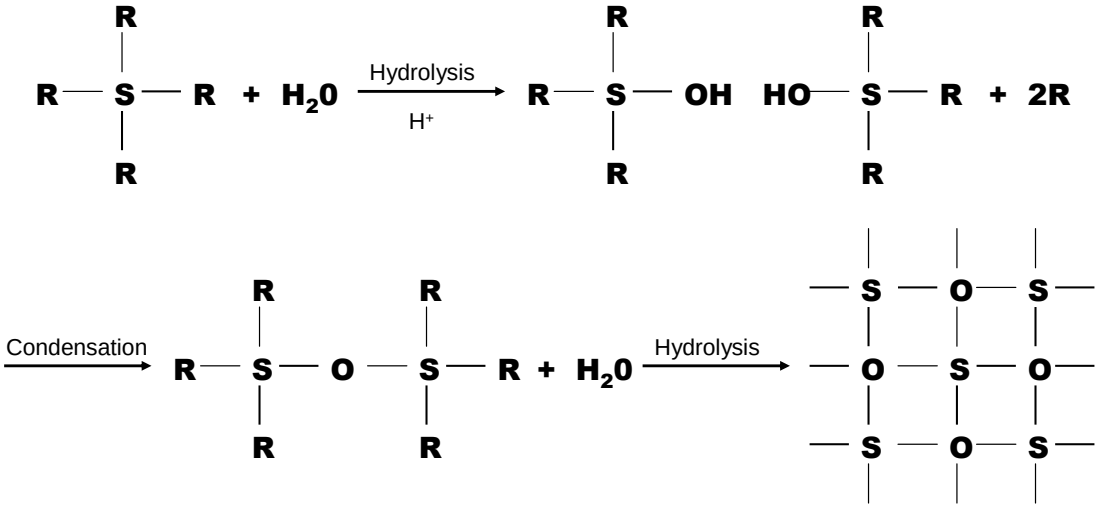

Figure 8 - Reaction mechanism used to create a silica network using TEOS and water in an acid catalyzed hydrolysis reaction.

The addition of a surfactant results in porous formation within the network. The micelles (as previously described) create interconnected pathways in the silica structure. A diagram of this formation can be seen in Figure 9.

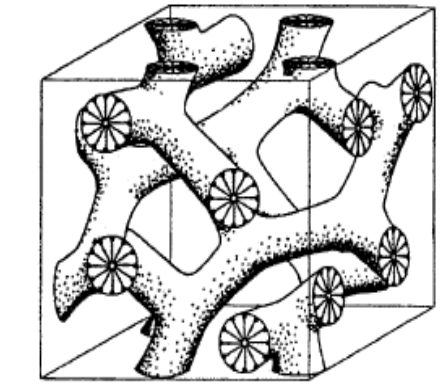

Figure 9 **-** Interconnected micellular structure found within silica structured inorganic membrane. Control of the micelle size provides for controlled pore size. [7]

The sol was created by adding 12.0g of 200 proof Ethanol to 5.41g deionized water. A solution of hydrochloric acid diluted to pH 2 with deionized water was added to the ethanol and water solution in a 5.4g portion. 10.4g of TEOS (tetraethylorthosilicate) was measured under nitrogen. The TEOS was added to the solution and stirred in a Parafilm covered beaker for 20 minutes.

Pluronic-123 (P-123) is a non-ionic surfactant produced in a paste form by BASF. The composition of this surfactant is a polyethylene oxide-polypropylene oxide-polyethylene oxide tri-block copolymer (PEO-PPO-PEO) [8]. Different amounts of surfactant were measured to create various weight percents of surfactant in the final solution (Please see Appendix B for calculations). The P-123 was measured in grams into a beaker. 200 proof ethanol was added to the P-123 at 8g. The silica solution (sol) was added to the Pluronic mixture and stirred in a Parafilm covered beaker until the surfactant was completely dissolved. The mixing period varied according to the amount of surfactant.

The dipping solution was left for periods ranging from 4 days to 1 week to complete adequate network formation. The extended time allowed for the silica solution to form around the Pluronic micelle network created in the sol. This formation created a solid structure to be plated on an appropriate substrate.

2.2.1.2 Deposition of Silica Sol-Gel

The sols were dipped on two different substrates. The first substrate was a porous alumina disk. These disks were prepared through the use of alumina powder. 3g of calcined alumina powder was measured into a prefabricated die. The die was pressed under 6500lbs of pressure for 8 minutes. The disk was carefully removed and examined for visible cracks and surface contamination. The disks were calcined at 600ºC for 3 hours. Each disk was hand polished using a combination of 15µm and 8µm grit diamond sandpaper.

The second substrate used for characterization purposes was a polished silicon single crystal. Each silicon substrate was cut from a larger silicon wafer using a diamond scribe. The wafers each measured approximately 1cm by 1.5 cm each. These substrates provided for a flat surface for deposition and allowed film thickness measurement.

The sols were dip coated using the apparatus shown in Figure 10. A thin layer of each sol was deposited on silicon wafers and an alumina disk at a constant rate. The sols were left to dry in a clean bench until the membrane had formed.

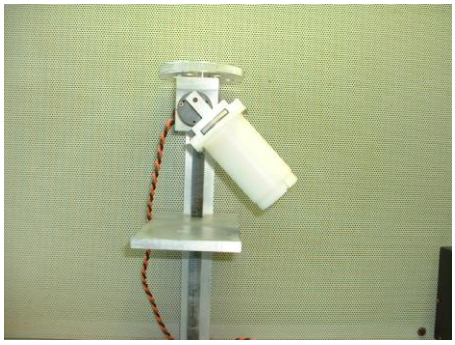

Figure 10 **-** Photograph of the dipping apparatus used to deposit silica sols on alumina and single crystal silicon substrates.

2.2.2 CHARACTERIZATION

Scanning Electron Microscopy (SEM) and x-ray diffraction were used to characterize the membranes. The SEM was used to determine the thickness of the membrane while indicating how evenly the film distribution occurred on the substrate. X-ray diffraction was used to indicate the arrangement of surfactant micelles in the membrane.

2.2.3 GAS PERMEATION

Gas permeation testing was conducted to characterize the membrane microstructurally using single gas measurements with oxygen, methane, nitrogen, argon, and helium. An alumina substrate silica plated membrane was placed in a gas permeance apparatus developed in the lab of Dr. William DeSisto of the University of Maine Chemical and Biological Engineering Department. The flow through the membrane was determined using a soap film flow meter. The pressure across the membrane was adjusted from 350-850 Torr to determine the permeance over a broad range of pressures. Temperature

ranges from 25-200ºC were tested to determine the relationship of permeance and pressure. These gases were forced through the porous disk while temperature, pressure, and flow rate were recorded. Membranes were tested both before and after the materials had been sintered.

2.3 Results and Discussion

The sols were created as explained in section 2.2.1.1 Creation of Silica Sol-gel. Visual characterization of the sols was completed upon formation and drying of the sol. It was found that smaller surfactant weight percent films (0.6-2.3wt%) were clear and brittle after drying. The higher surfactant weight percent films (6.5-13.9wt%) were found to become cloudy upon drying and were flexible. These results were kept in mind during future testing.

The SEM was used to determine the thickness of the film that was deposited on a single crystal silicon substrate. The edge of the film was used to determine the thickness. Figure 11 is an SEM picture of a 1.1wt% surfactant film.

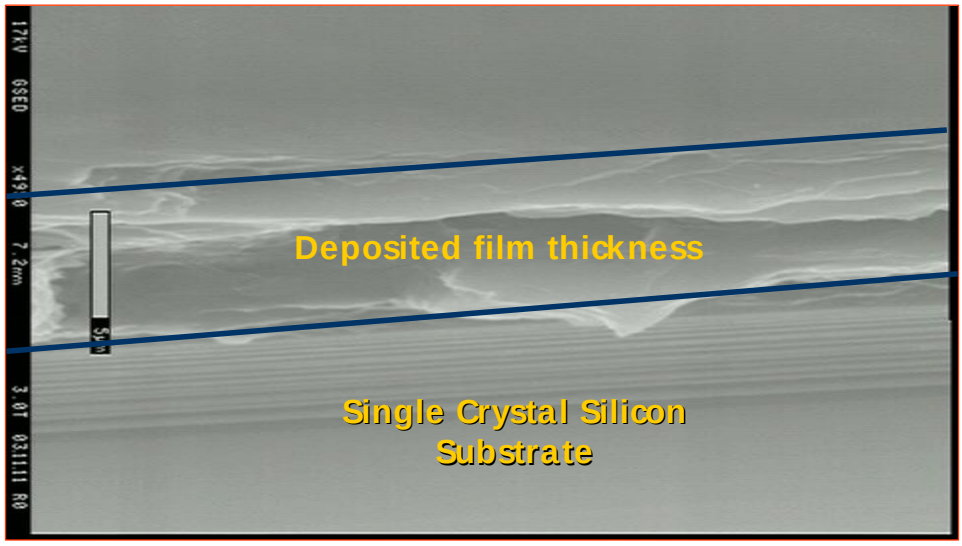

Figure 11 – SEM picture of a 1.1wt% surfactant silica thin film deposited on a crystal silicon substrate. This picture indicates the film thickness through the use of the SEM measurement at approximately 5µm.

The SEM measurements indicated that the film deposition thickness was approximately 5µm. This thickness was found to change slightly with different surfactant concentrations but remained in the same range. The SEM indicated that the lower weight percent surfactant films were very thin. These films in the 1µm range showed cracking and chipping indicating that the low surfactant concentration did not have adequate network formation in the film.

Gas permeance was used to characterize the blank alumina disks and the porous silica films. Sols were created from surfactants concentrations varying from 0.6-13.9wt%. These surfactant concentrations were analyzed to determine their individual properties. An example of this analysis will be presented using a 2.3wt% surfactant film that was

dipped after four days. Other graphs of substrate characterization can be found in Appendix C. The blank disk was characterized separately to create baseline data. Nitrogen gas was used to permeate the disk. Figure 12 indicates the relationship of permeance versus pressure for a blank 3g alumina disk after four days of sol formation.

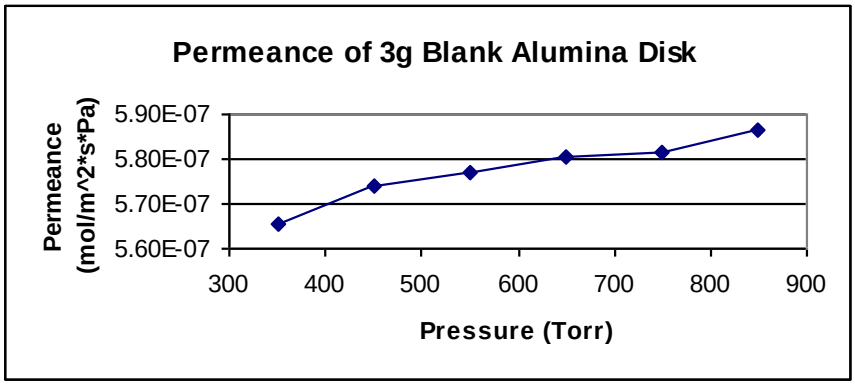

Figure 12 – Permeance data for blank alumina disk. This permeance data provides a baseline to relate to the silica film that will be deposited on the surface. The disk was later dipped in a 2.3wt% surfactant film.

As the pressure of the gas is increased the permeance of the disk increases. The total permeance differential was found to be $2.1*10^{-8}$ $mol*m^{-2}s^{-1}Pa^{-1}$. This dependence on pressure indicates that the pores of the disk lie in the macroporous range characterized by viscous flow in Equation 3. The disk was then dip-coated in a 2.3wt% surfactant sol. Gas permeance was used to test the pre-calcined silica film. Nitrogen and helium gases were not found to penetrate the film. The lack of permeation in the disk indicates that the film was relatively free of deformities and contamination. If these defects had been observed a significant gas flow would have been observed.

Calcination of the disk was performed to remove the surfactant molecules leaving a porous structure for gas particles to flow. Nitrogen gas was used to determine the

permeance readings for the film and disk. The change in permeance from 350-850 Torr was $1.6*10^{\wedge -8}$ $mol*m^{-2}s^{-1}Pa^{-1}$. Figure 13 displays a graph of the flow properties through the 2.3wt% surfactant silica film and alumina disk.

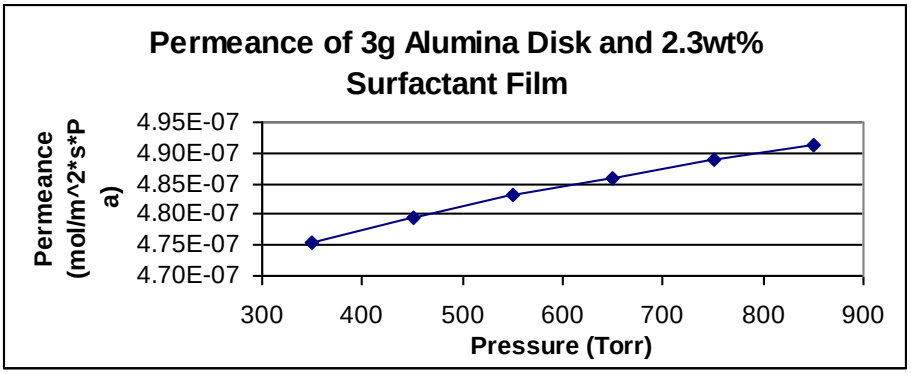

Figure 13 – Permeance versus pressure data for the 2.3wt% surfactant silica film and the porous alumina support.

The value of the film permeance can be determined by subtracting off the blank disk permeance. This was accomplished using Equation 9. The resulting values were plotted in Figure 14.

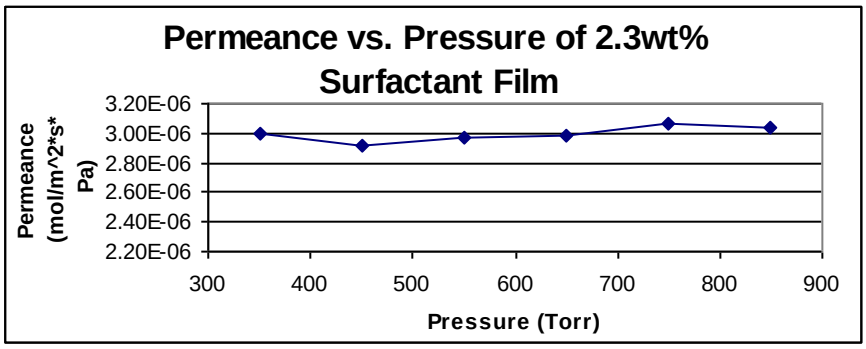

Figure 14 – Permeance vs. pressure data for the 2.3wt% surfactant silica film. This was calculated using Equation 9 by subtracting off the permeance of the blank disk.

The data for the permeance of the film indicated that the flow had no apparent dependence on pressure signifying that Knudsen flow was demonstrated. Permeance values in the 10^{-6} range also indicated that the pores are interconnected. A lack of pressure dependence indicated that the pores lie in the mesoporous range. All permeance data for the blank disk, disk and film, and film were plotted and can be seen in Figure 15.

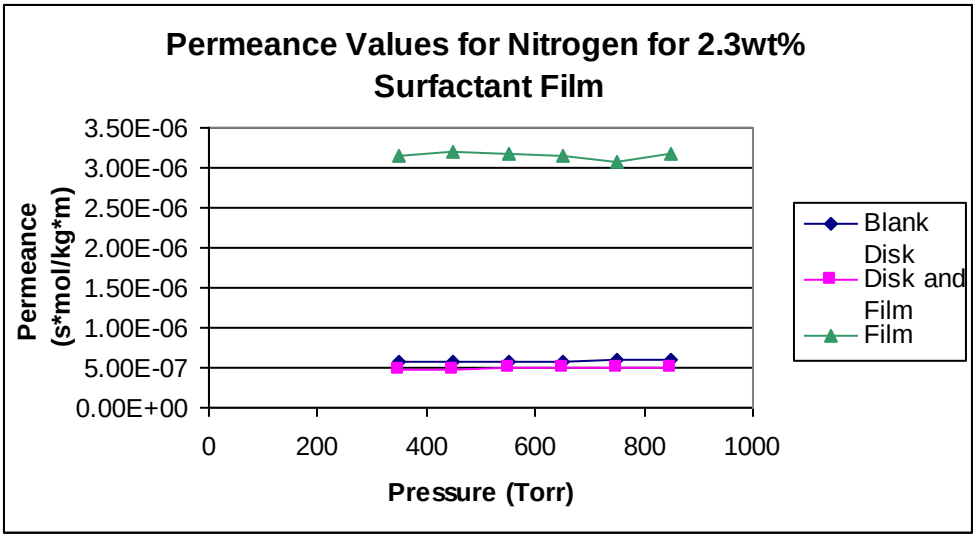

Figure 15 - Permeance vs. pressure comparison between blank disk, film and disk, and the film of 2.3wt% surfactant. The results indicate that an increased permeance can be seen in the film.

The comparison indicates that the film has a higher permeance than the blank disk. This is characteristic of a thinner film due to the decrease in thickness.

The films of different surfactant concentrations were found to have different permeance values. Additional surfactant concentration should provide for increased micelles to form within the solid but may interfere with proper formation of the silica backbone network.

Figure 16 presents a chart of 0.6, 2.3, 10.3 and 13.9 weight percent surfactant concentrations.

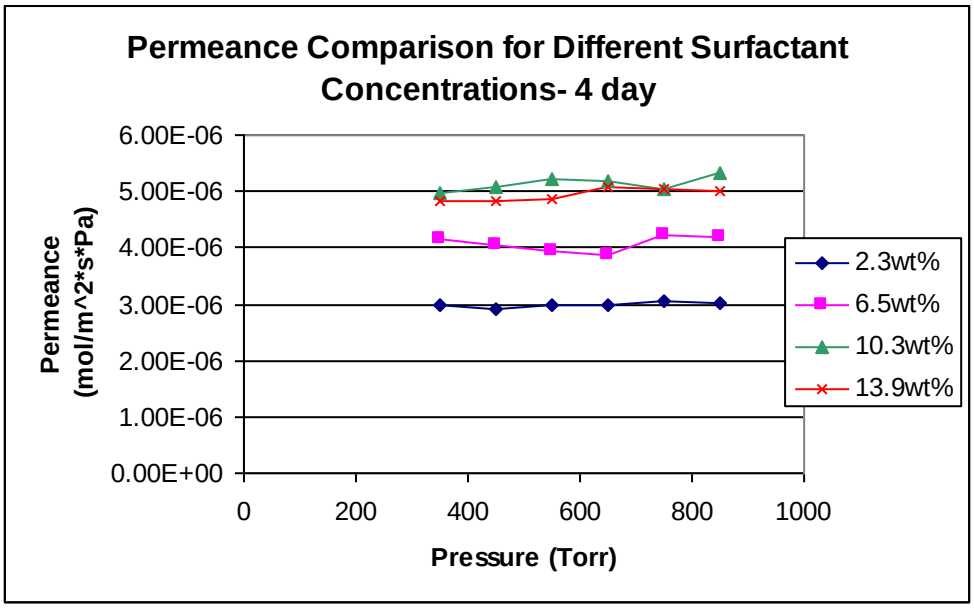

Figure 16 - Permeance vs. pressure for four surfactant weight percent concentrations of surfactant. Permeance values were found to increase with increasing weight percent concentration.

The data obtained from all the different surfactant concentrations indicates that as the surfactant concentration is increased the permeance through the film increases. When analyzing the higher weight percent concentrations it can be seen that the 10.3 and 13.9wt% surfactant films had similar permeance values. A possible cause of the results is that defects may have been present in the films prepared using high surfactant concentrations. The lower weight percent films were analyzed further.

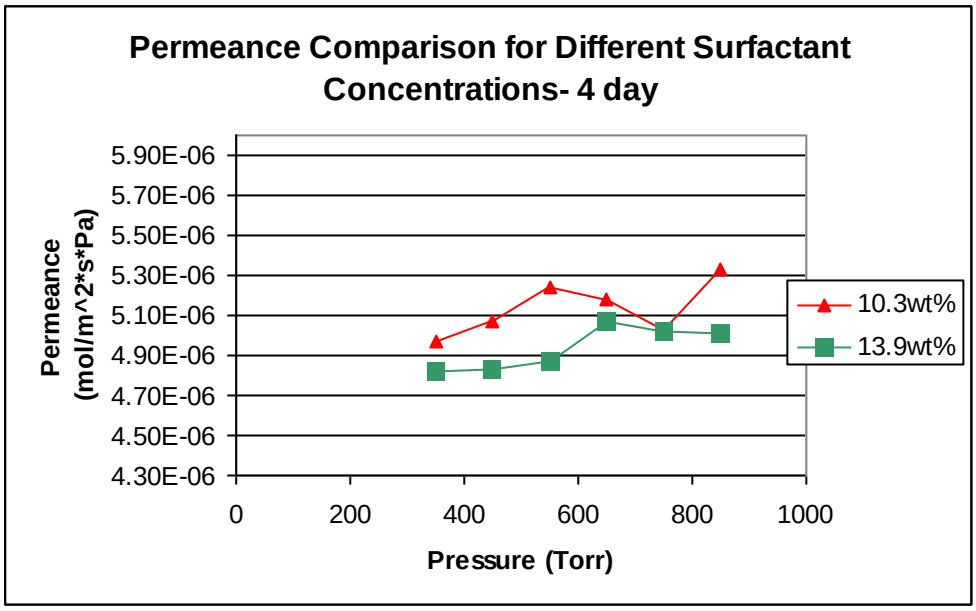

Figure 17 - Permeance vs. pressure for four surfactant weight percent concentrations of surfactant. Permeance values were found to increase with increasing weight percent concentration.

Upon closer inspection of the 10.3 and 13.9wt% surfactant films it was observed that a slight dependence on pressure may have occurred. This dependence on pressure may have been due to defects occurring in the macroporous range. As a result of this data it was determined that that films of lower surfactant concentrations would be used in further testing.

A test was completed to determine if a sol that was left for an extended period of time before dipping would have a better network formation. The sols that had been dipped after four days were left to form for an additional three days. These sols were then dipped using the same procedure as had been completed previously. Figure 18 presents the permeance data for a seven day film at 6.5wt% surfactant concentration.

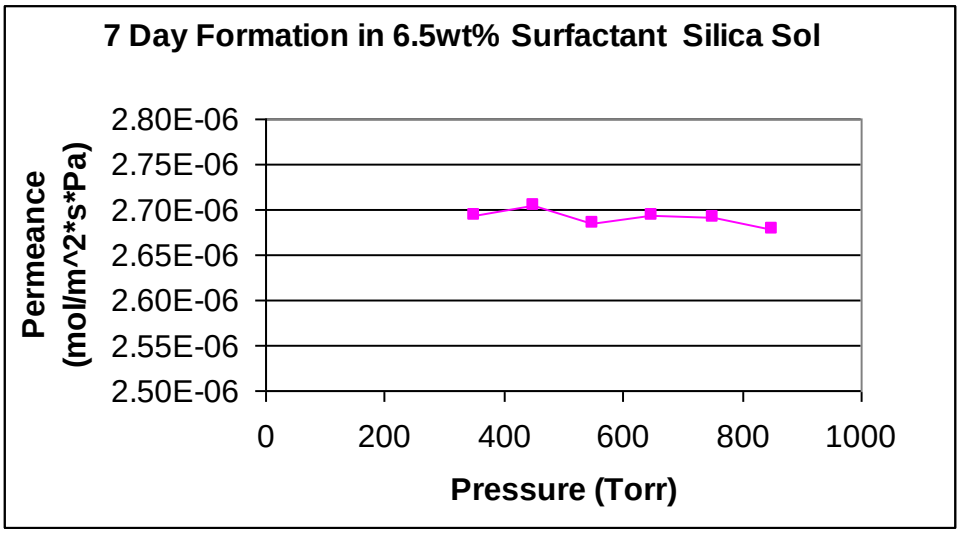

Figure 18 **-** Permeance vs. pressure for a 6.5wt% surfactant film plated 7 days after formation of the sol**.**

The permeance data obtained for the four day and seven day periods were compared to determine if a greater network formation had taken place during the longer standing time of the sol. It was found that a small decrease in permeance was observed in the seven day film. In comparison, the decrease in permeance was also followed by a more uniform correlation as the pressure increased. Figure 19 presents a comparison of this data.

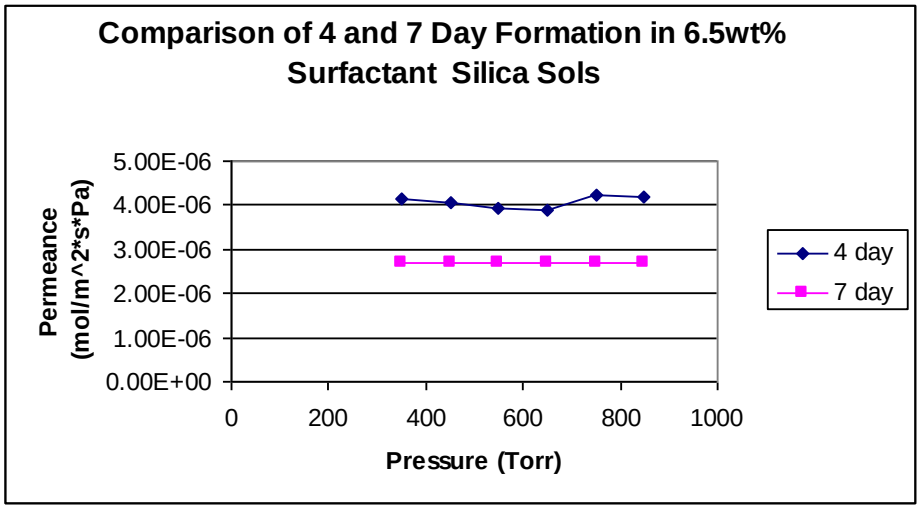

Figure 19 – Permeance versus Pressure for the 6.5wt% surfactant silica films dipped at 4 and 7 days. Decreased permeance values were seen for the extended 7 day formation period.

The same correlation was found for all surfactant weight percent films. It was determined that a more uniform permeance was of greatest importance. Therefore, all subsequent experiments used 7-day films. The additional data on these films can be found in Appendix D.

The temperature dependence of the membranes was tested using the gas permeance unit. Membranes with surfactant weight percents of 0.6, 1.1, 2.3, and 6.5 wt% were examined at temperatures ranging from 25-200ºC and with a variety of gases as shown in Table 1. The flux through the membrane was calculated using Equation 5. It was anticipated that lower molecular weight gas molecules would have a larger flux within the membrane.

Table 1 – Table of gases and their molecular weights (MW) used in the gas permeance unit to determine the flux versus molecular weight at different temperatures.

Gas	MW (gm/mol)
He	4.002602
Me	16.03452
N2	28.013
O2	31.999
Ar	39.948

Each disk was tested and the results were plotted. The data for the 2.3wt% surfactant film are seen in Figure 20. Additional data for other films can be found in Appendix E.

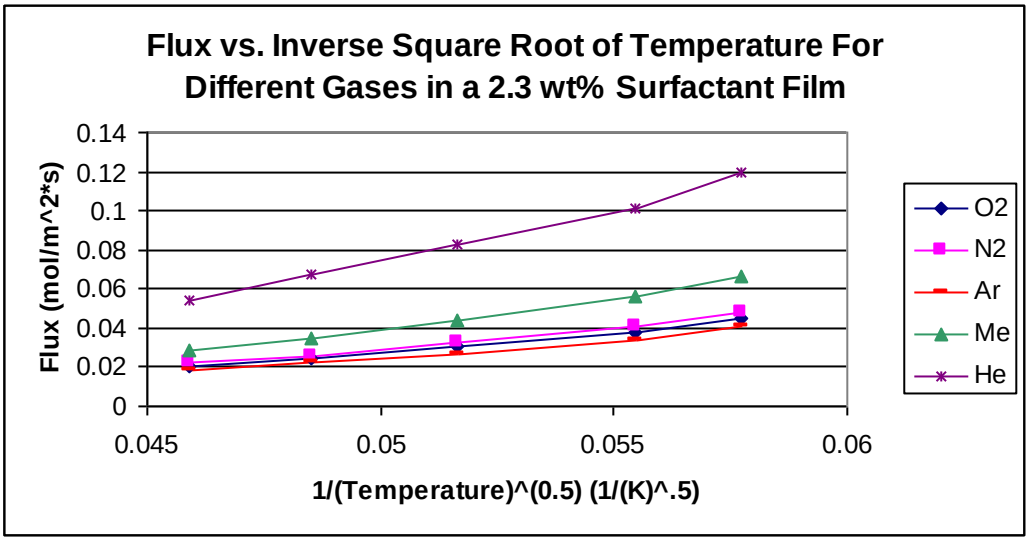

Figure 20 – Flux versus the Inverse Square Root of Temperature for a 2.3wt% surfactant film with different gases each used in single gas permeation.

Flux values were found to increase with decreasing molecular weight. Since flux is a measure of the rate of flow per unit area, smaller molecules should be able to proceed through the membrane at a higher rate. In terms of temperature dependence, it was observed that the flux through the membrane increases with the inverse square root of temperature. In terms of kinetic energy, the gas molecules will be moving faster as the temperature increases. From equation 8 it can be observed that there is an inverse

relationship between the flux and temperature. This relationship can be observed in this data and the graphs for other weight percent surfactant films presented in Appendix E.

A second comparison was made between flux and molecular weight. It was determined according to equation 8 that at a constant temperature the flux through the membrane should be proportional to the square root of the molecular weight of a gas. Figure 21 presents that gas flow data for a 2.3wt% surfactant film.

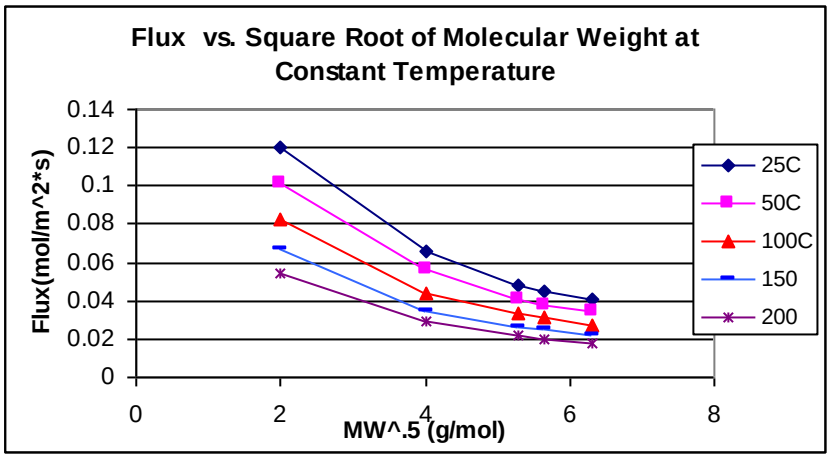

Figure 21 – Flux versus the Square Root of Molecular Weight - at constant temperature for a 2.3wt% surfactant film with different gases used in single gas permeation.

The data indicates that as the square root of the molecular weight of the gas increases the flux through the membrane decreases. This relationship further confirms the Knudsen Flow through the membrane.

2.4 Conclusions

- Mesoporous silica membranes were prepared using a non-ionic micellular templating technique. A non-ionic block copolymer, Pluronic 123, formed micelles that directed the hydrolysis and condensation of TEOS. The membranes were formed by removing the template by thermal decomposition leaving behind a porous structure with pore size estimated to be 5nm.

- The membranes were approximately 5μm thick and coated on porous alumina disks.

- The silica membranes were prepared with varying amounts of template. It was found that for template surfactant concentrations in the range of 0.6-13.9wt% that N_2 permeance was on the order of approximately $3*10^{-6}$ $mol*m^{-2}s^{-1}Pa^{-1}$. An independence of permeance and pressure drop was measured indicating Knudsen Flow.

- The permeace of different gases varied inversely to molecular weight further consistent with Knudsen Flow.

2.5 Recommendations

- Continue the study of sols created using different weight percent surfactants. Particular attention should be focused on higher weight percent films.

- Perform gas chromatograpy on all sols. The gas chromatography will determine the separation properties of the membranes.

- Further characterize the membrane pore formation through x-ray diffraction analysis. X-ray diffraction will help to determine the pore formation and will provide for more insight into the results obtained during testing.

3. Synthesis and Characterization of Microporous Gold Nanoparticle Membranes via Langmuir-Blodgett Deposition

3.1 Introduction

The idea of using gold nanoparticles as the sole composition for a membrane is an untouched field. The ability to create gold nanoparticles was accomplished by Enustun and Turkevich in 1963. Since this time further study has been completed. Studies completed at the University of Cambridge by Kawai et al. that indicated gold nanoparticles can provide a multi-layered structure when compressed in a Langmuir-Blodgett trough beyond the monolayer. The hypothesis of this experiment was that the ability to plate this multi-layer on an appropriate surface could provide for the formation of a membrane.

In this study the targeted size of gold nanoparticles is 15nm. Based on packing calculations, this size of particle would provide a pore formation with a diameter of 2.3nm. This pore size lies on the boundary between mesoporous and microporous character. Pore diameter calculations for different particle sizes can be found in Appendix A.

The application for these membranes is yet to be determined. It is anticipated that these membranes could have potential use in industrial applications and may even become of use in the medical field. Further investigation into the membranes may provide for insight into this area.

3.2 Experimental

3.2.1 SYNTHESIS

3.2.1.1 Creation of Gold Nanoparticle Subphase

The nanoparticles were synthesized according to a standard citrate reduction technique [17,18]. Anhydrous citric acid at 99.5% purity (Alfa Aesar) and hydrogen tetrachloroaurate at 99.9% purity (Alfa Aesar) were employed in the reaction.

The reaction was performed in 1.5 liter portions to provide enough solution for the experiment. An addition of 0.1g $HgAuCl_4$ was made to 800mL deionized water in a large Erlenmeyer flask. The solution was heated to 70°C while maintaining vigorous stirring. An addition of 0.4g of citric acid was made to 200mL of deionized water and heated in a separate beaker to 70°C under vigorous stirring conditions. Both solutions were monitored with thermometers and the containers covered with aluminum foil.

After both solutions had reached 70ºC the citric acid solution was added to the $HgAuCl_4$ solution. This new solution was continuously stirred and maintained at a constant temperature for 3 hours. After this time the solution was left to cool to room temperature while maintaining constant stirring. The solution then appeared red indicating nanoparticle sizes were in an anticipated range of 15±2 nm [14].

3.2.1.2 Deposition of Gold Nanoparticles

The nanoparticles were plated on substrates using a Langmuir-Blodgett trough as described by Kawai et al. Figure 24 indicates the set-up of the Langmuir-Blodgett Trough.

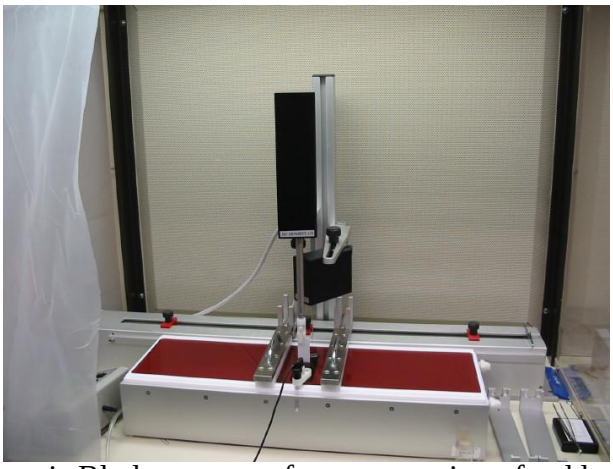

Figure 22 – Langmuir-Blodgett set-up for compression of gold nanoparticles at the air-subphase interface

The trough was thoroughly cleaned before deposition using Micron-90 soap solution and soft-bristled brushes. After deposition the trough was cleaned with Aqua Regia, and chloroform. The gold nanoparticles present in a subphase filled the trough in 1.5L amounts. A solution of $1x10^{-3}$M dioctadecyldimethylammonium chloride (DODAC) in chloroform solution was spread over the subphase-air interface in 90µL amounts using a microsyringe. The solution was left for 10 minutes to allow for the evaporation of the chloroform from the interface. After this time a film of nanoparticles had formed on the air-subphase interface. The resulting film was compressed at a rate of 10mm/min. As indicated by Kawai et al., the film should be compressed to a surface pressure of 40mN/m to obtain a monolayer. The film was compressed to 43 mN/m to initiate rafting

of the layers. As the compression progressed the surface became gold and metallic in appearance. This compressed film was allowed to sit for 24 hours to provide for maximum formation of the layer.

The particles were plated on the substrate at an approximately horizontal angle. This was completed by raising the substrate through the interface surface at a rate of 2mm/min. The plated layer was left stationary until dry to prevent contaminating the deposition.

3.2.2 CHARACTERIZATION

SEM and gas permeation were used to characterize the membranes. The SEM was used to determine the thickness of the membrane and indicate how evenly the film distribution was on the substrate. Gas permeation testing was used to provide data for permeance, flux, and temperature using different gases.

3.2.3 GAS PERMEATION

Gas permeation testing was completed using single gas measurements of nitrogen. An alumina substrate plated membrane was placed in the gas permeance apparatus. The flow through the membrane was measured with a soap film flow meter. The pressure across the membrane was varied from 350-850 Torr to determine the permeance over a broad range of pressures. Temperature ranges from 25-200ºC were tested to determine the relationship of permeance and pressure. These gases were forced through the porous disk

while temperature, pressure, and flow rate were recorded. The permeance of the nanoparticle film was calculated from the total measured permeance using equation 8.

3.3 Results and Discussion

The characterization of the nanoparticles began during the synthesis. As indicated in the literature the particles can be characterized by the color solution that results [15]. Gold nanoparticles in the 15±2 range are characterized by a red solution. The red solution resulted after approximately one minute of stirring the reactants and was preceded by blue and purple colors. This red solution results from the mean free path of the electrons in the solution.

Isotherms were recorded during compression of the gold nanoparticles on the surface of the Langmuir-Blodgett Trough. The isotherms indicated the barrier position versus the surface pressure on the air-subphase interface. As the particles were compressed the surface pressure increased due to the decreased surface area available for each particle. An isotherm created from data taken during the dipping of a .5g surfactant alumina disk can be seen in Figure 25.

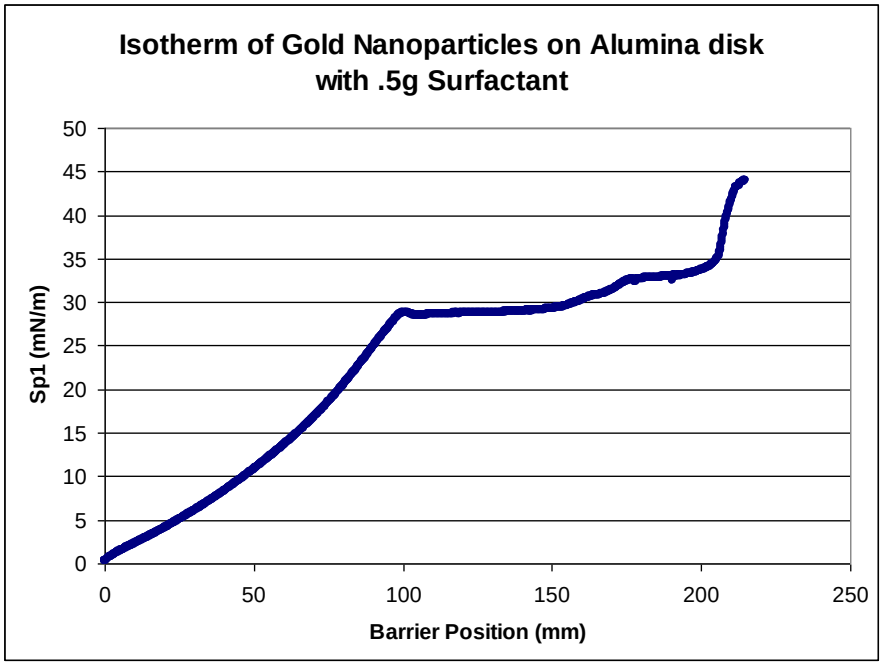

Figure 23 – Isotherm of compression of 15nm gold nanoparticles in a Langmuir-Blodgett Trough

The figure indicates that the compression of the particles occurs in a relatively exponential manner. It displays that there are two distinct points of change from the exponential compression. One point occurs at a barrier position of 100 mm and the second at a position of 200 mm. These points are the result of phase changes occurring in the film. Due to prior experimentation by Kawai et al. it was known that the monolayer would be reached at 40 mN/m. It was anticipated that compression beyond this point resulted in the rafting of the monolayer forming a multi-layered structure. This effect can be seen upon closer examination of the isotherm. After the surface pressure reached 44 mN/m the pressure began to jump. This compression and decompression was due to the decreased surface tension caused by the layering of the particles as they collapsed into a multi-layered structure.

The SEM was used to investigate the visual and physical aspects of the deposited gold nanoparticle multi-layer. These SEM images indicated that the particles were forming in a layered manner along the support. The images indicated little contamination and fairly homogeneous coverage of the support. These images indicate that the compression to form the layer went beyond the point of mono-layer compression to begin rafting of the particles. An SEM image of a multi-layer film can be seen in Figure 26.

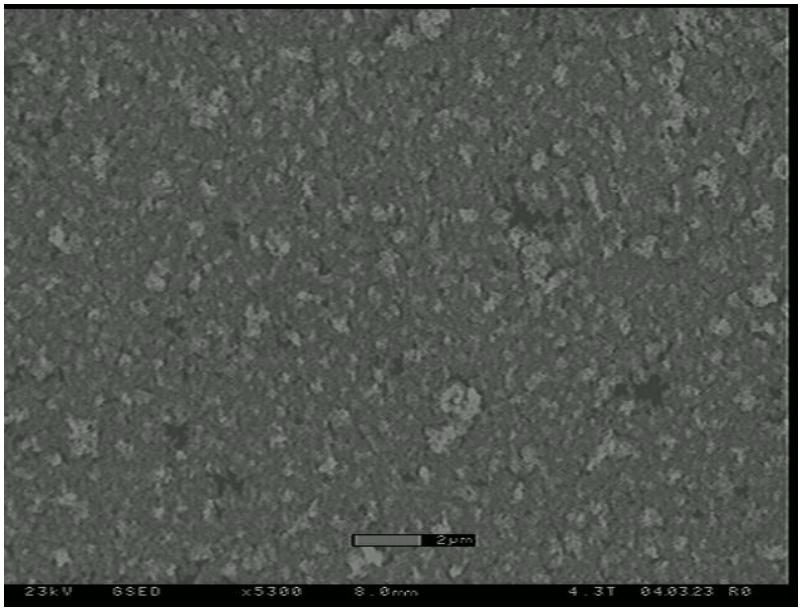

Figure 24 –Scanning Electron Microscope image taken of silicon disk plated with and multi-layer of 15nm gold nanoparticles.

After the plating on bare silicon supports indicated that multi-layer deposition of gold nanoparticles had occurred the particles were plated on alumina supports with silica plated films. SEM taken from these plates indicate that multi-layer formation of gold nanoparticles occurred over the silica membranes.

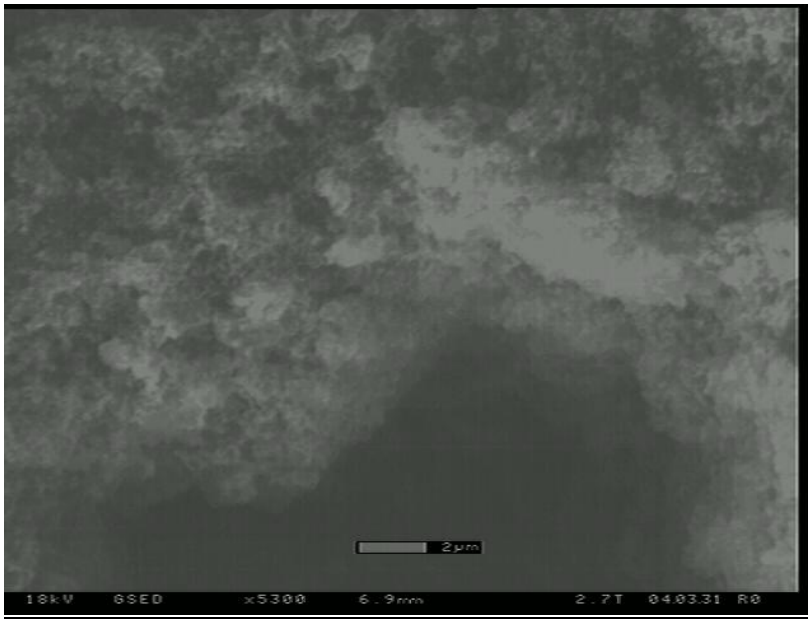

Figure 25 – SEM picture taken on the 1.1wt% disk from 2/26/04. The picture indicates that mountainous structures formed during compression of the multi-layer. These layers successfully deposited on the plated silica support.

Gas permeance testing was completed on the membranes. The same methods for testing were applied as have been previously described. The permeance through the membranes was found to be higher than that through the silica membranes or alumina disk. This indicates that a very thin layer of gold nanoparticles resulted. Figure 28 presents the permeance versus pressure values for nitrogen through one of the films plated on a 2.3wt% surfactant silica film.

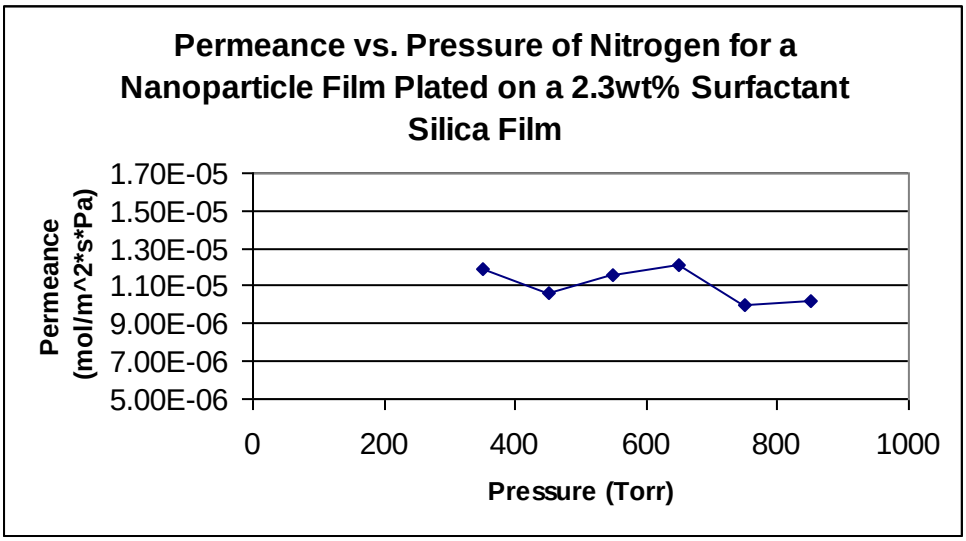

Figure 26 –Permeance versus Pressure of nitrogen for a 15nm nanoparticle film plated on a 2.3wt% surfactant silica film.

The values indicate a permeance in the range of $1.19*10^{-5}$ $mol*m^{-2}s^{-1}Pa^{-1}$with nitrogen gas. The greatest change in permeance for the different pressures was found to be $2.0*10^{-6}$ $mol*m^{-2}s^{-1}Pa^{-1}$. These values do not show a dependence on pressure indicated that the pore formation is in the microporous or mesoporous range.

A comparison was made between the permeance of the nanoparticle film and the silica support. Figure 29 presents the permeance of the gold nanoparticle film in comparison to the permeance of the silica film and alumina support.

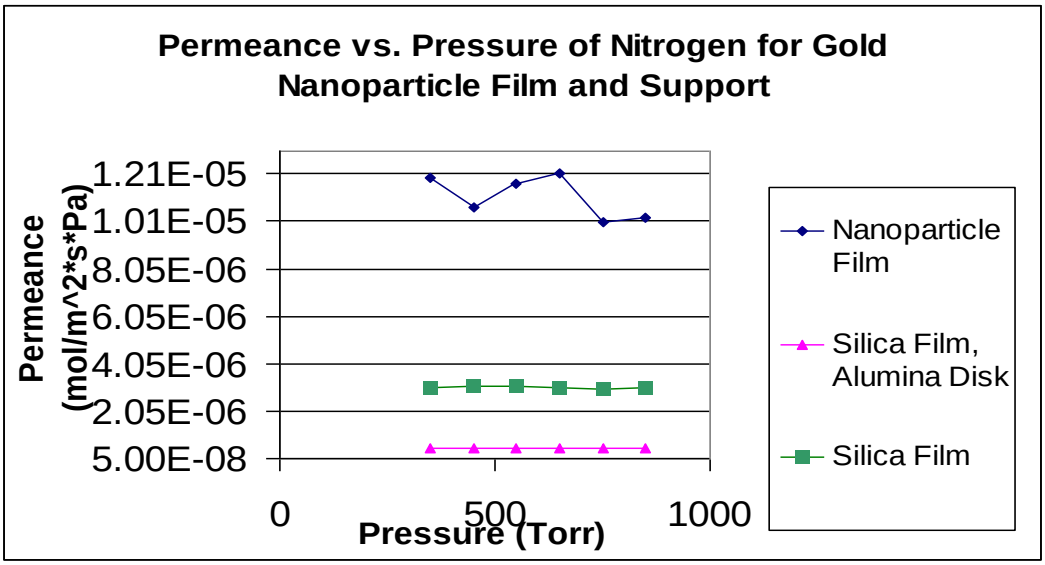

Figure 27 –Permeance versus Pressure of nitrogen for a 15nm nanoparticle film and 2.3wt% surfactant film, and the silica film and alumina disk combined.

The permeance for the film was found to be $1.12*10^{-5}$ $mol*m^{-2}s^{-1}Pa^{-1}$ higher than the support. The nanoparticle film had a permeance that was $8.58*10^{-6}$ $mol*m^{-2}s^{-1}Pa^{-1}$ higher than that of the 2.3wt% surfactant film. This data indicates that a very thin nanoparticle layer was deposited in on the silica support resulting in a high permeance.

Another plated disk was used to determine if the results of the experiment were reproducible. Figure 30 presents the data from two different nanoparticles films.

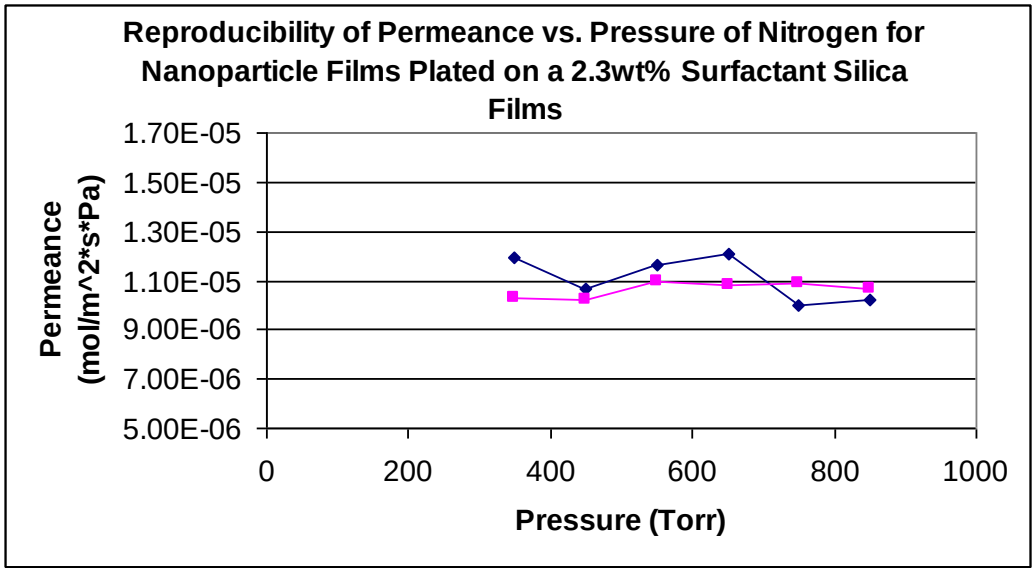

Figure 28 – Reproducibility of Permeance versus Pressure of nitrogen for 15nm nanoparticle films plated of 2.3wt% Surfactant Silica Films

The permeance results indicate that the films are very similar in permeance characteristics. Both films lie in the range of $1.19*10^{-5}$ $mol*m^{-2}s^{-1}Pa^{-1}$. This data indicates that the gold nanoparticle films are reproducible.

3.4 Conclusions

- A novel synthesis method based on the controlled layer-by-layer deposition of spherical gold nanoparticles that had specific particle size and shape was investigated.

- Silica membranes serve as a good support for gold nanoparticle plating. The films were found to hold up during plating and provided the necessary support structure for nanoparticle deposition.

- Scanning Electron Microscopy on the gold nanoparticle plated silicon and alumnia disks indicated that a multi-layered packing arrangement was present in the membrane structure

- Compression Isotherms indicated that a multi-layer structure was formed on the trough air-subphase interface. The fluctuating surface pressure in the trough indicated that there was a significant rafting of the particles occurring.

- The gold nanoparticle membranes form a thin layer that is characteristic of a high permeance through the membrane.

- The permeance through the membrane was higher than that of the silica films. This indicates a very thin film providing for high flux through the membrane.

- This novel synthesis method has promised for the controlled synthesis of ultrathin (<100 nm) microporous membranes with controlled pore size based on the interparticle spacing created by the close packing nanoparticle structure.

3.5 Recommendations

- Continue gas permeance testing on the membranes to further characterize separation properties. Other gases and temperatures may be used to determine flux relationships.

- Perform further testing to determine if the gold nanoparticle pore formation lies in the microporous range. It is anticipated that the surface structure can be further characterized by advanced imaging techniques. Further testing of porisimetry and gas separation will provide more evidence of pore formation.

- Create nanoparticles of different sizes and deposit on suitable silica membranes. Nanoparticles of different diameters may provide for different separation properties due to the size of pore formation. Further investigation may indicate more opportunities.

- Further investigate potential uses for gold membranes. The application of gold nanoparticles is yet to be determined but may find some relevance in a variety of fields.

Works Cited

1) Burggraaf, A. J., Co, L.; Fundamentals of Inorganic Membrane Science and Technology, Elsevier Science B.V. The Netherlands, 1996

2) Bischoff, B. L.; Membranes and Their Uses. Inorganic Membrane Technology Laboratory, 2002. Ref. Feb 15, 2004. http://www.inorganicmembranes.info/uses.html

3) Xomeritakis, G., Naik, S., Braunbarth, C.M., Cornelius, C.J., Pardey, R., Brinker, C.J.; *Journal of Membrane Science*. **2003**, 215, 225-233

4) Narayan, R.K., Anderson, M.T., Brinker, C.J, *Chem. Mater*. **1996**, 8, 1682-1701

5) Geankoplis, Christie J. *Transport Processes and Unit Operations*. Prentice HALL PTR, Englewood Cliffs, New Jersey, 1993

6) Neilson, Daniel L. and Cox, Michael M. *Lehninger Principles of Biochemistry*, Third Edition, 2002

7) Ramen, N. K., *Chem. Mater*. **1996**, 8, 1682-1701

8) Alberius, P. C., *Chem. Mater*. **2002**, 14, 3284-3294

9) Dobkin, Daniel M., *Pressure, Size and Knudson Numbers*. Ref. 3/20/04. www.batnet.com/.../ xprt/Knudsen.html

10) Fain, Douglas E., *Development of Inorganic Membranes fir Gas Separation*. Ref. 2-10-04. http://www.ornl.gov/sci/fossil/Publications/RECENT%20PUBS/imtl.pdf

11) Williams, G.A., CWP and Regents of the University of California; *Agnes Pockels* Updated 10/13/97. Ref. 3/5/04 http://www.physics.ucla.edu/~cwp/Phase2/Pockels,_Agnes@871234567.html

12) KSV Instruments LTD. KSV 2000 Instruction Manual. Helsinki, Finland

13) Journal of Chemical Education; *Agnes Pockels*. Ref. 3/8/04. http://jchemed.chem.wisc.edu/JCEWWW/Features/eChemists/Bios/pockels.html

14) Kawai, T.; Neivandt, D. J.; and Davies, P. B. *J. Am. Chem. Soc.* **2000**, 122, 12031-12032

15) Sauls, Barbara L.; Sauls, F. C. Close Packed Structures. 1998, Ref. Jan. 12, 2004. http://www.kings.edu/~chemlab/vrml/clospack.html,

16) McCool, Benjamin A. *Synthesis and Characterization of Microporous Silica Membranes Fabricated Through Pore Size Reduction of Mesoporous Silica Membranes Using Atomic Layer Deposition*. University of Maine, 2003

17) Enustun, B.V.; Turkevich, J. *J. Am. Chem. Soc.* **1963**, 85, 3317.

18) Slot, J. W.; Geuze, H. J. *E. J. Cell Biol*. **1985**, 38, 87

Appendices

Appendix A
Pore Diameter Calculations

Layered Gold Nanoparticles Space Calculations

Using 30-60-90 triangles, I was able to solve for the radius of a particle that could fit in between the gold nanoparticles assuming they are perfect spheres and rest snugly together in a layered form.

t - variable used in reference to the 30-60-90 particles.
R - the variable used for the radius of the gold nanoparticle
r - the variable for the radius of the particle of interest
d - diameter for the radius of the particle of interest

15 nm particles $nm := 10^{-9}m$

$R := \frac{15nm}{2}$

$t := \frac{R}{\sqrt{3}}$

$r := 2t - R$ $r = 1.16nm$ $d := 2 \cdot r$ $d = 2.321nm$

20 nm particles $nm := 10^{-9}m$

$R := \frac{20nm}{2}$

$t := \frac{R}{\sqrt{3}}$

$r := 2t - R$ $r = 1.547nm$ $d := 2 \cdot r$ $d = 3.094nm$

30 nm particles $nm := 10^{-9}m$

$R := \frac{30nm}{2}$

$t := \frac{R}{\sqrt{3}}$

$r := 2t - R$ $r = 2.321nm$ $d := 2 \cdot r$ $d = 4.641nm$

50 nm particles $nm := 10^{-9}m$

$R := \frac{50nm}{2}$

$t := \frac{R}{\sqrt{3}}$

$r := 2t - R$ $r = 3.868nm$ $d := 2 \cdot r$ $d = 7.735nm$

Appendix B
Solution Weight Percent Calculations

Solution Weight Percent Calculations

$dTEOS := .933\frac{gm}{cm^3}$ $WtTEOS := 10.4cm^3 \cdot dTEOS$ $WtTEOS = 9.703 \times 10^{-3} kg$

$SolWTwoSur := 5.4gm + 5.4gm + 12gm + WtTEOS + 8gm + 3gm$ $SolWTwoSur = 0.044kg$

.25 g Surfactant

$PointTwoFivewt\% := \frac{.25gm}{SolWTwoSur + .25gm} \cdot 100$ $PointTwoFivewt\% = 0.571$

.5 g Surfactant

$PointFivewt\% := \frac{.5gm}{SolWTwoSur + .5gm} \cdot 100$ $PointFivewt\% = 1.136$

1 g Surfactant

$Onewt\% := \frac{1gm}{SolWTwoSur + 1gm} \cdot 100$ $Onewt\% = 2.247$

3 g Surfactant

$Threewt\% := \frac{3gm}{SolWTwoSur + 3gm} \cdot 100$ $Threewt\% = 6.451$

5 g Surfactant

$Fivewt\% := \frac{5gm}{SolWTwoSur + 5gm} \cdot 100$ $Fivewt\% = 10.309$

7 g Surfactant

$Sevenwt\% := \frac{7gm}{SolWTwoSur + 7gm} \cdot 100$ $Sevenwt\% = 13.861$

Appendix C
Permeance Data

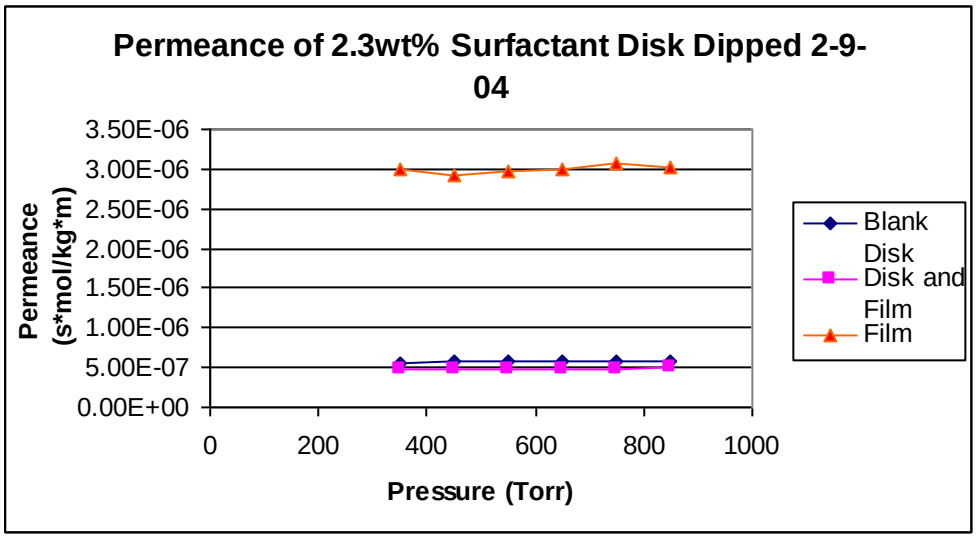

Figure 29 - Permeance vs. pressure comparison between blank disk, film and disk, and film of a 2.3wt% surfactant film. The results indicate that a increased permeance can be seen in the film.

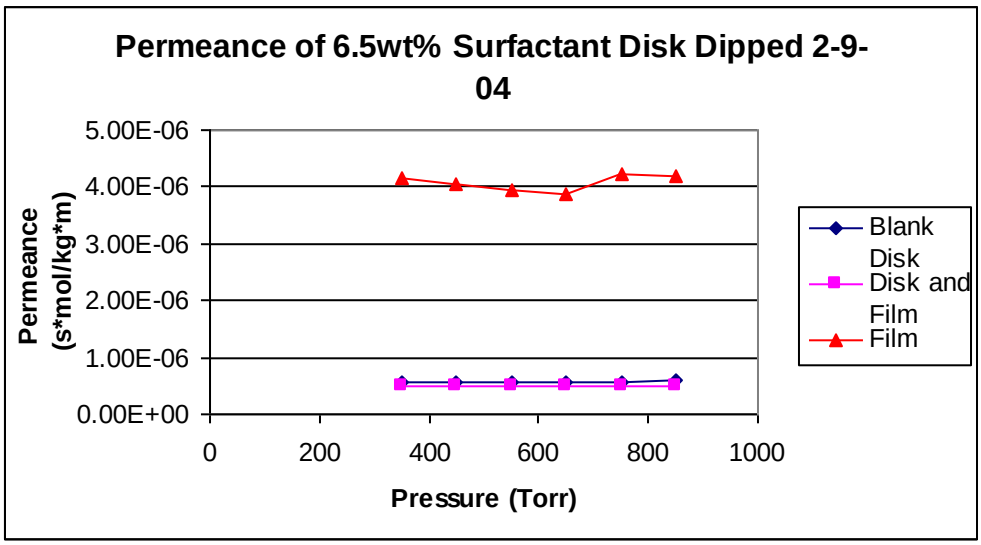

Figure 30 - Permeance vs. pressure comparison between blank disk, film and disk, and film of a 6.5wt% surfactant film. The results indicate that a increased permeance can be seen in the film.

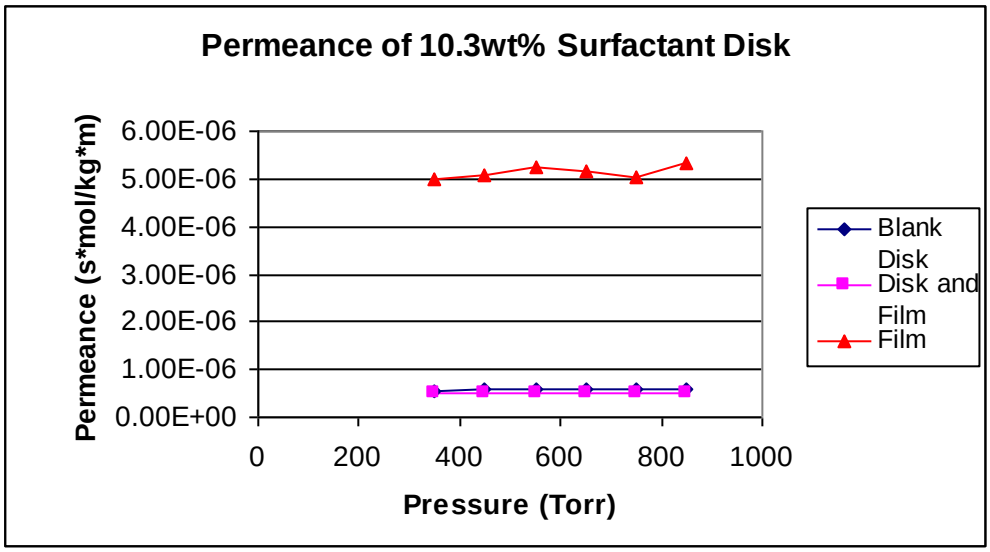

Figure 31 - Permeance vs. pressure comparison between blank disk, film and disk, and film of a 10.3wt% surfactant film. The results indicate that a increased permeance can be seen in the film.

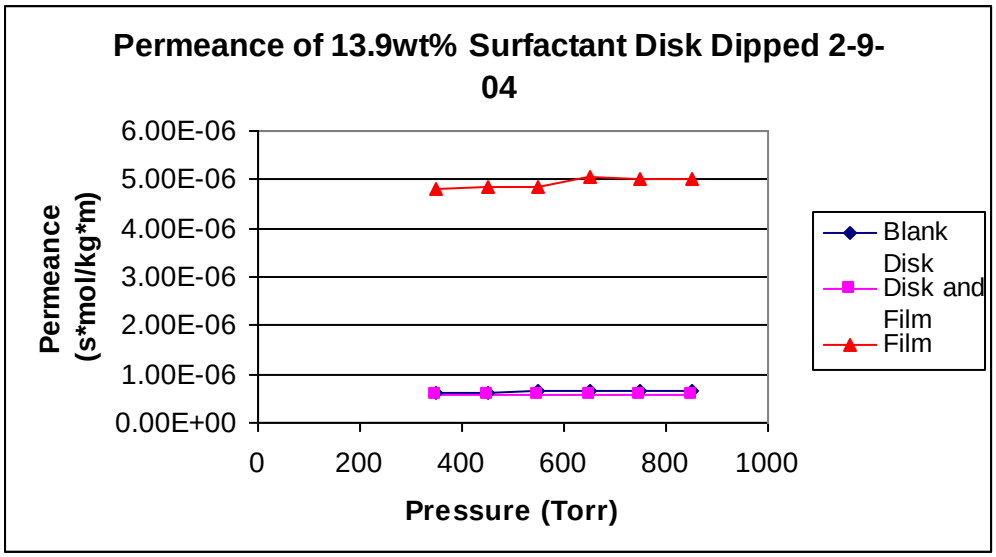

Figure 32 - Permeance vs. pressure comparison between blank disk, film and disk, and film of a 13.9wt% surfactant film. The results indicate that a increased permeance can be seen in the film.

Appendix D
4 and 7 Day Sol Formation Comparison

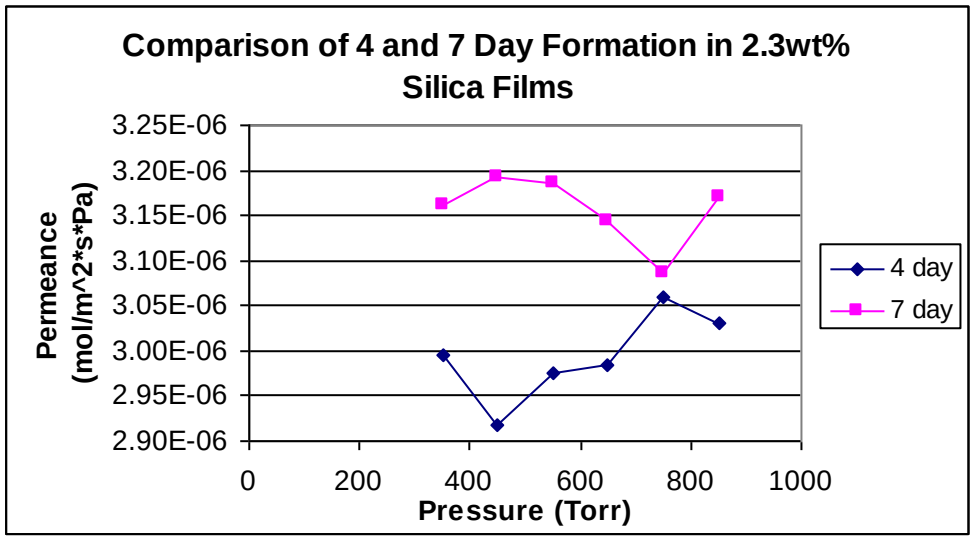

Figure 33 **-** Permeance vs. pressure for a 2.3wt% surfactant film plated 4 and 7 days after formation of the sol.

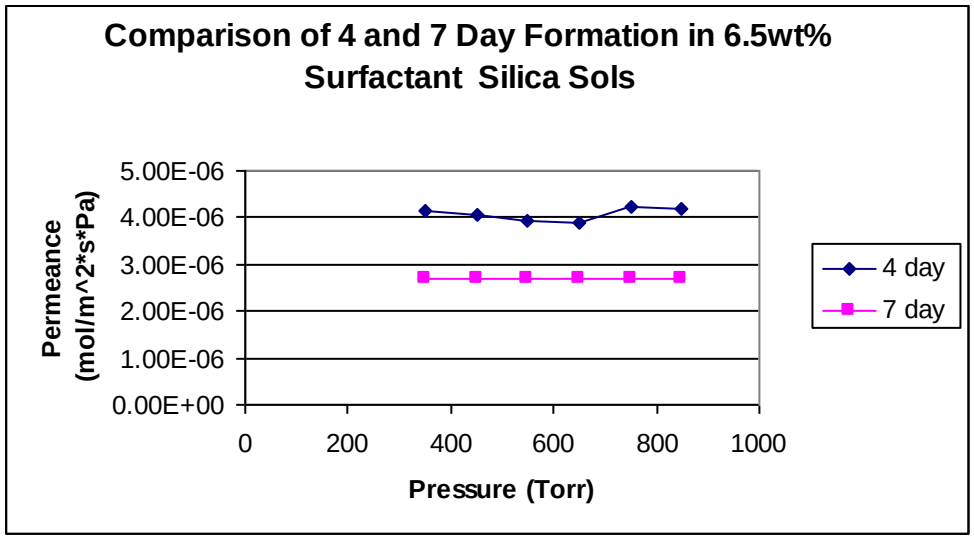

Figure 34 **-** Permeance vs. pressure for a 6.5wt% surfactant film plated 4 and 7 days after formation of the sol.

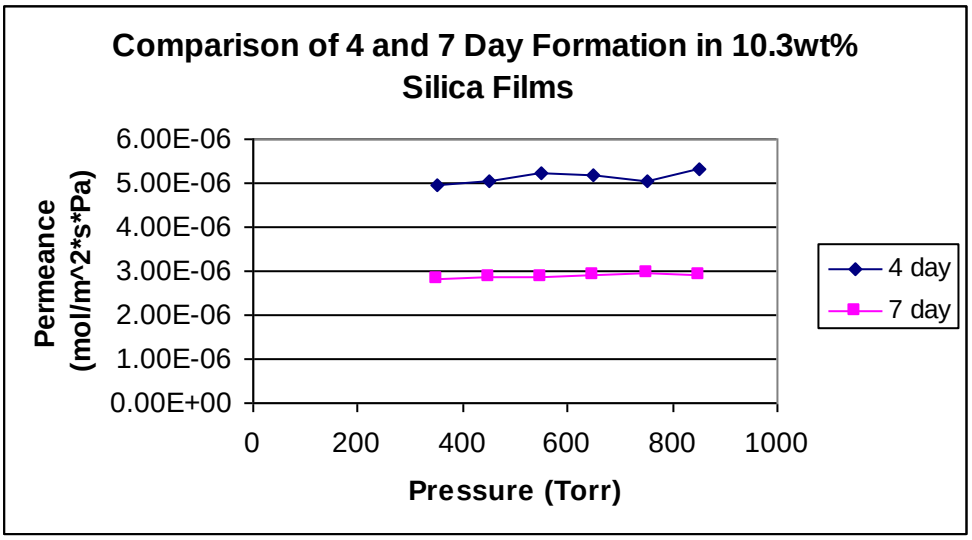

Figure 35 - Permeance vs. pressure for a 10.3wt% surfactant film plated 4 and 7 days after formation of the sol.

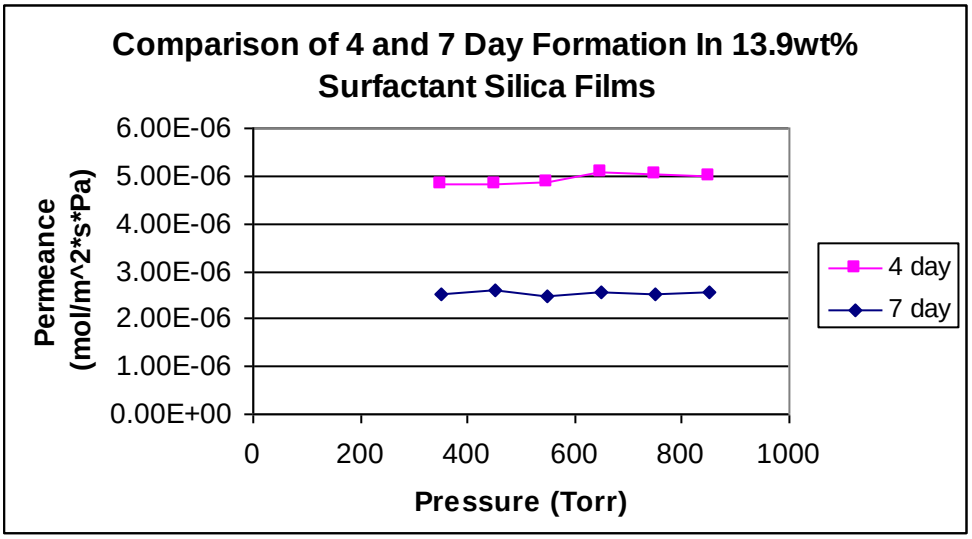

Figure 36 - Permeance vs. pressure for a 13.9wt% surfactant film plated 4 and 7 days after formation of the sol.

Appendix E
Flux versus Inverse Square Root of Temperature

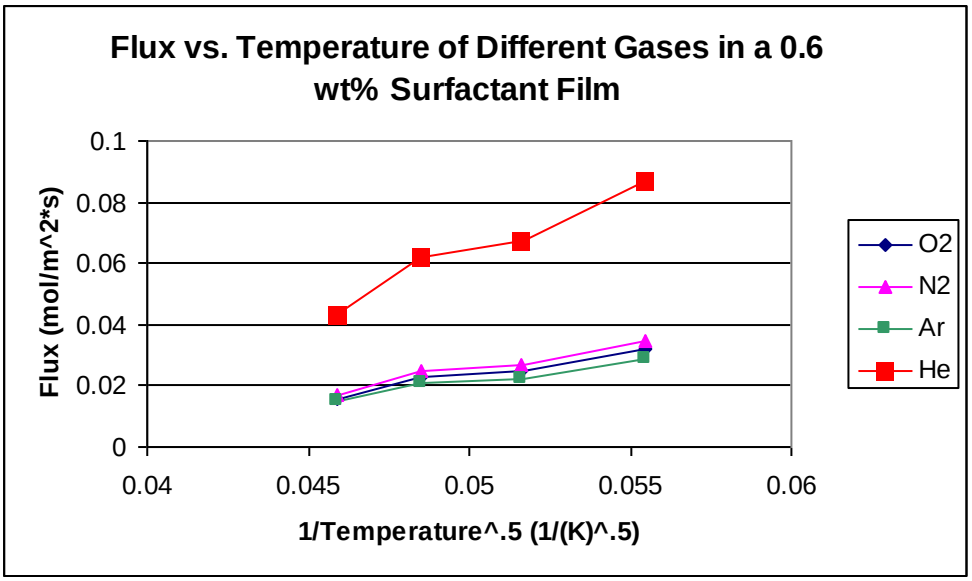

Figure 37 – Flux versus Temperature for a .6wt% film with different gases each used in single gas permeation.

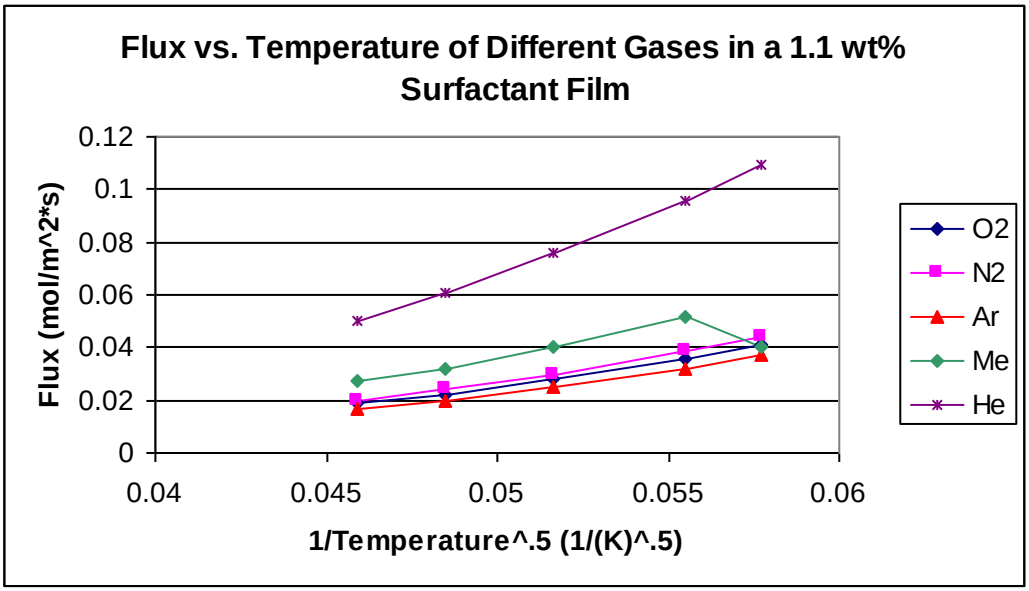

Figure 38 – Flux versus Temperature for a 1.1wt% film with different gases each used in single gas permeation.

Biography of the Author

Jennifer Saucier was born in Millinocket, Maine on September 18, 1981. Jennifer graduated from Stearns High School in 2000 as Valedictorian and Class President. Jennifer attended the University of Maine in Orono where she completed a B.S. degree in Chemical Engineering and Honors with minors in Pre-Medical Studies and Chemistry. While at school she held offices in the UMaine Student Alumni Association, AICHE, TAPPI-PIMA. Jenny was also involved in various honor societies such as Tau Beta Pi and Golden Key. She plans to further her education by attending medical school in the fall of 2005.